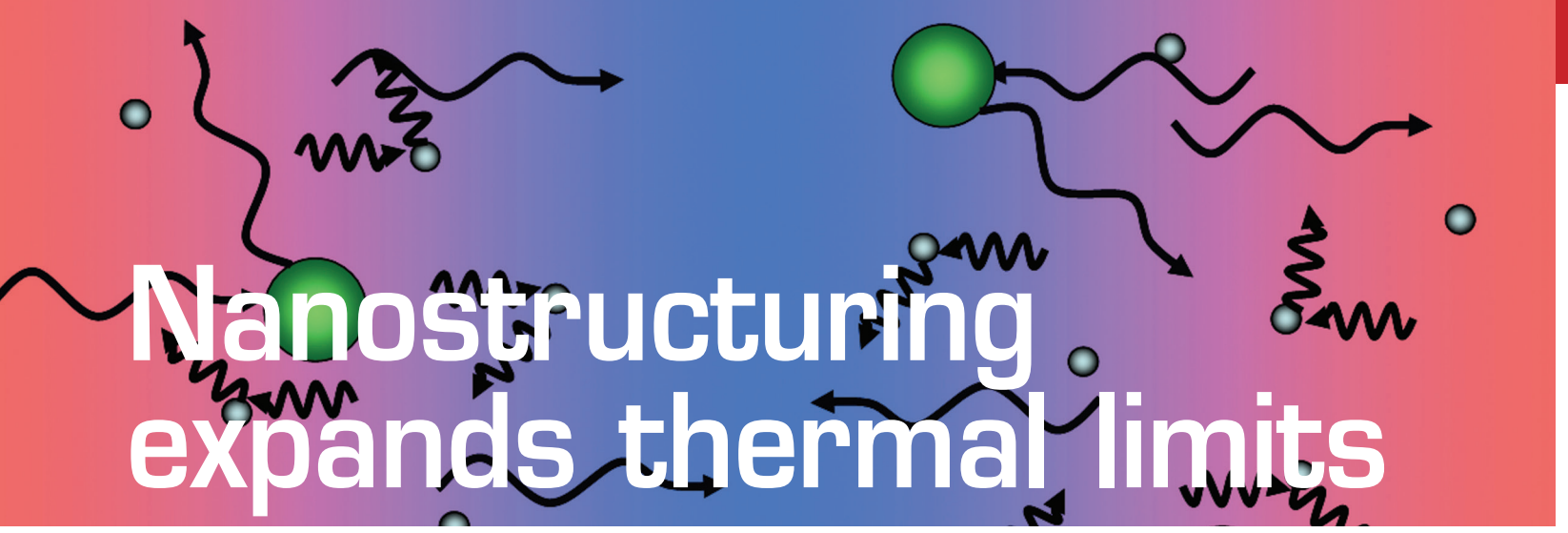

# Nanostructuring expands thermal limits

**Scientists and engineers can exploit nanostructures to manipulate thermal transport in solids. This is possible because the dominant heat carriers in nonmetals – crystal vibrations (or phonons) – have characteristic lengths in the nanometer range. We review research where this approach is used and propose future research directions. For instance, concepts such as phonon filtering, correlated scattering, and waveguiding could expand the extremes of thermal transport in both the insulating and conducting limits. This will have major implications on energy conservation and conversion, information technology, and thermal management systems.**

**Woochul Kim[1], Robert Wang[1], and Arun Majumdar[1,2]***

*[1]Department of Mechanical Engineering, University of California, Berkeley, CA 94720, USA*

*[2]Materials Sciences Division, Lawrence Berkeley National Laboratory, Berkeley, CA 94720, USA*

**E-mail: majumdar@me.berkeley.edu*

**Since the discovery of electricity, research on charge transport in materials has pushed the extremes of electrical conductivity, which now spans over 20 orders of magnitude. Five decades ago, the invention of the transistor demonstrated external tuning of electrical conductivity and formed the foundation for information processing and the digital age.**

The societal impact of research on electrical conduction is clearly enormous. In contrast, thermal transport in materials has received less attention. The thermal conductivity of current solid materials at room temperature spans only four orders of magnitude. Yet, the history of thermal transport goes back to primitive humankind who combined empirical observations with applications (specific heat of stone for warmth, straw for insulation, wooden tools for manipulating fire, etc.).

Recent research on thermal transport in nanostructures has expanded the extremes of thermal transport in both the insulating and conducting limits. If we push the extremes far enough, the technological ramifications will be significant. Thermal management of integrated circuits is the biggest challenge in microelectronics today[1]. The most promising way to push magnetic data storage to 1 TBit/in$^2$ is through thermally assisted magnetic recording in Co-based nanostructures[2]. Because of a phonon bottleneck, it is difficult to increase the frequency range of GaN microwave devices beyond 100 GHz[3]. Ultralow thermal conductivity materials can be used for thermal barrier coatings in jet engines[4], whereas extremely high thermal conductivities can be used for heat sinks[5]. Also, if one can design materials with ultralow thermal conductivity, and high electrical conductivity and thermopower, it may be possible to develop high-efficiency thermoelectric refrigerators and power generators[6]. This article reviews recent research that has broken the thermal transport limits by nanostructuring, and proposes future research directions.



ISSN:1748 0132 © Elsevier Ltd 2007

There are two types of heat carriers in solids: electrons and crystal vibrations (or phonons). This review focuses on nonmetallic materials where phonons are the dominant carrier. A phonon is a quantum of crystal vibrational energy and is analogous to the photon[7]. Just as a solid radiates out a Planck-like distribution of photons, it also contains a Planck-like distribution of phonons within itself[8]. Phonons have two fundamental lengths: wavelength and mean free path[7]. At room temperature, the dominant heat-carrying phonons typically have wavelengths of 1-3 nm and mean free paths of 10-100 nm. By using nanostructures comparable in size to these length scales, one can then manipulate thermal transport in solids[9,10].

Fig. 1 shows possible approaches to increase the range of thermal conductance and conductivity. The range of thermal conductivity at room temperature spans four orders of magnitude: from polymers at ~0.1 W/mK to diamond at ~$10^3$ W/mK. Phonon transport in these materials is diffusive and the phonon scattering events are uncorrelated. In this article, we focus on a broader range of phonon transport mechanisms such as spectrally dependent scattering, phonon filtering, correlated scattering, waveguiding, and ballistic transport. In the case of phonon filtering and correlated scattering (e.g. localization), it may be possible to prevent a spectral band(s) from propagating, thereby reducing thermal conductivity. On the other hand, waveguiding and ballistic transport can increase the thermal conductance significantly.

## The thermally insulating limit

In this section, we review work that pushes the insulating limits in thermal transport. For example, we discuss how researchers beat the alloy and amorphous limits by nanostructuring. Recent reports on phonon filtering and correlated scattering are also reviewed.

### The alloy limit

The lowest thermal conductivity $k$ in crystalline solids is generally that of an alloy and is often referred to as the 'alloy limit'. Alloys have low thermal conductivity because the atomic substitutions heavily scatter phonons. This is known as alloy scattering. Thermal conductivities of alloys are typically 5 W/mK < $k$ < 10 W/mK at room temperature. Historically, it has been difficult to beat the alloy limit without creating defects, dislocations, and voids. However, by using nanostructures such as superlattices[11,12], nanowires[13], and nanoparticles[14,15], researchers have been able to beat the alloy limit. In some cases[13,15], these nanostructures provide a scattering mechanism other than alloy scattering, such as spectrally dependent phonon scattering. In alloys, atomic substitutions scatter phonons because of differences in mass and/or bond stiffness. In the Rayleigh scattering regime, the scattering cross-section varies as $\sigma \sim b^6/\lambda^4$ where $b$ is the size of the scattering particle and $\lambda$ is the phonon wavelength. Since atomic substitutions in alloys have $b \sim 1$ Å, this relation suggests that alloys scatter short-wavelength phonons much more effectively than mid- and long-wavelength phonons. Hence, these latter phonons dominate heat conduction in alloys. If one introduces another scattering mechanism that scatters mid- and/or long-wavelength phonons, the alloy limit can be beaten. Nanostructuring is one way of achieving this. Two examples are presented here – an alloy-based nanowire[13] and an alloy containing nanoparticles[15]. In nanowires, long-wavelength phonons are scattered by the nanowire boundaries, i.e. boundary scattering[16], whereas in a bulk material containing nanoparticles, mid- to long-wavelength phonons are scattered by nanoparticles[17-19] in the material.

Fig. 2a shows thermal conductivities of 58 nm and 83 nm diameter single-crystalline $Si/Si_xGe_{1-x}$ superlattice nanowires and a $Si_{0.9}Ge_{0.1}$ alloy film for comparison[13]. The thermal conductivity of the nanowire is clearly below that of the alloy film. The thermal conductivity reduction is most pronounced in the low temperature regime and negligible at room temperature. Recognizing that long-wavelength phonons dominate thermal transport in the low temperature regime, this thermal conductivity trend is a key signature of boundary scattering[7] by the $Si/Si_xGe_{1-x}$ superlattice nanowire.

Another example of beating the alloy limit by using spectrally dependent phonon scattering is shown in Fig. 2b. By introducing epitaxially embedded ErAs nanoparticles into an $In_{0.53}Ga_{0.47}As$ alloy, short-wavelength phonons are scattered by the $In_{0.53}Ga_{0.47}As$ alloy and mid- and long-wavelength phonons are scattered by the

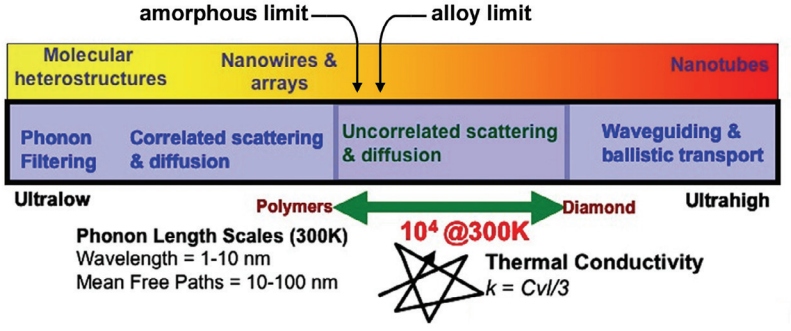


*Fig. 1 Schematic illustrating various approaches to expand the limits of thermal transport. This can be accomplished with nanostructured materials, which can tune into the phonon wavelength and mean free path.*

ErAs nanoparticles[15]. Fig. 2b shows the thermal conductivity of $In_{0.53}Ga_{0.47}As$ with randomly distributed ErAs nanoparticles and an $In_{0.53}Ga_{0.47}As$ alloy for comparison. Once again, the alloy limit is beaten by using nanostructures, in this case, ErAs nanoparticles. The inset shows the phonon mean free path with respect to frequency at 300 K for $In_{0.53}Ga_{0.47}As$ with and without ErAs nanoparticles. As shown, the mean free path of mid- to long-wavelength phonons has been suppressed, indicating ErAs nanoparticles preferentially scatter those phonon wavelengths. The theoretical analysis used in Fig. 2b assumed specular reflection at the interface between the ErAs nanoparticle and the $In_{0.53}Ga_{0.47}As$ matrix. Since the ErAs nanoparticles are epitaxially embedded in $In_{0.53}Ga_{0.47}As$, the interface roughness is small compared with the phonon wavelength and the assumption of specular interface should be valid. Diffuse scattering should be applicable to nonepitaxially embedded nanostructures. Theoretical studies on nanowire/nanoparticle-based composites assuming diffuse interface scattering are available elsewhere[20-23]. Irrespective of whether the interface is specular or diffuse, a large interface area per unit volume containing a nanostructure is preferable to reduce thermal conductivity of the nanocomposite[20,24].

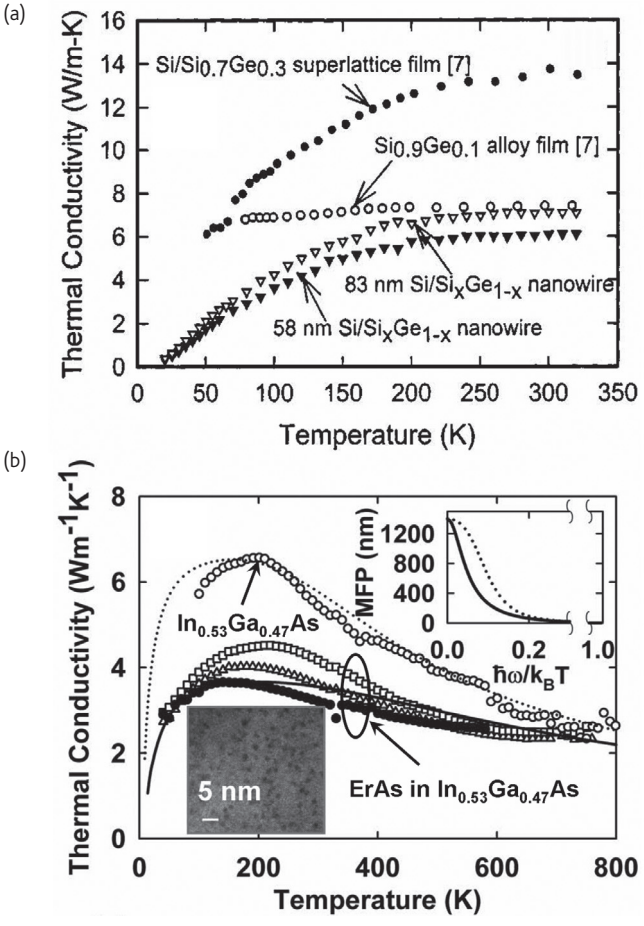


*Fig. 2 (a) Thermal conductivities of 58 nm and 83 nm diameter single-crystalline $Si/Si_xGe_{1-x}$ superlattice nanowires. The value of x is ~0.9-0.95 and the superlattice period is 100-150 nm. Thermal conductivities of a 30 nm period two-dimensional $Si/Si_{0.7}Ge_{0.3}$ superlattice film and $Si_{0.9}Ge_{0.1}$ alloy film (3.5 μm thick) are also shown. (b) Thermal conductivity of randomly distributed ErAs in $In_{0.53}Ga_{0.47}As$ (solid circles). Thermal conductivity of an $In_{0.53}Ga_{0.47}As$ alloy (open circles), 0.4 monolayer with a 40 nm period thickness $ErAs/In_{0.53}Ga_{0.47}As$ superlattice (open squares), and 0.1 monolayer with a 10 nm period thickness $ErAs/In_{0.53}Ga_{0.47}As$ superlattice (open triangles) are shown as references. Dotted and solid lines are based on theoretical analysis. The transmission electron micrograph inset shows randomly distributed ErAs in $In_{0.53}Ga_{0.47}As$. The inset graph shows the phonon mean free path (MFP) versus normalized frequency at 300 K. (Part (a) reprinted with permission from[13]. © 2003 American Institute of Physics. Part (b) reprinted with permission from[15]. © 2006 American Institute of Physics.)*

## The amorphous limit

Amorphous solids do not exhibit long-range crystalline order[7]. This disorder destroys coherence of lattice vibrations and limits the mean free path to a few lattice spacings at most. This causes extremely low thermal conductivity and is often referred to as the amorphous limit. Thermal conductivities of amorphous oxides fall in the range 1.3 W/mK < *k* < 3.0 W/mK at room temperature[25].

Since the mean free path in an amorphous solid is already extremely small, beating this limit by further reducing the mean free path is not viable. Costescu *et al.*[25] beat the amorphous limit by using a material with a high interface density, a $W/Al_2O_3$ nanolaminate. The $W/Al_2O_3$ nanolaminate is a thin-film multilayer where each layer is only a few nanometers thick. In this material, they found that interfaces dominate the thermal conductance. The thermal conductivity of the $W/Al_2O_3$ nanolaminate is shown in Fig. 3. Data for an $Al_2O_3$

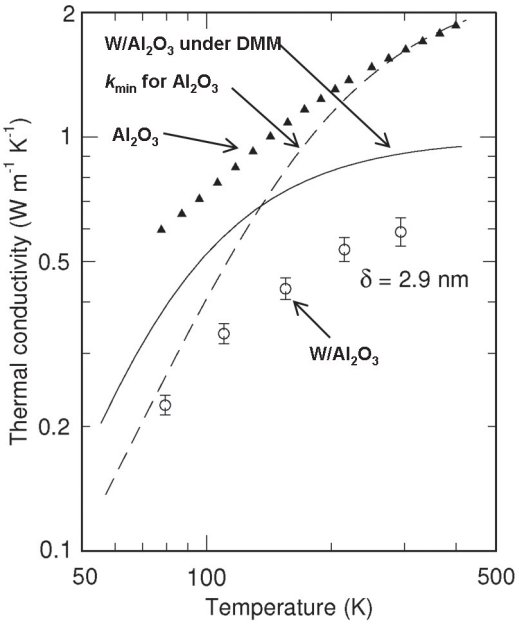


*Fig. 3 Thermal conductivity of the $W/Al_2O_3$ nanolaminate as a function of temperature. The nanolaminate interface spacing δ is 2.9 nm. Data for an $Al_2O_3$ film, the calculated $Al_2O_3$ minimum conductivity $k_{min}$, and DMM[26] analysis of the $W/Al_2O_3$ nanolaminate are shown for comparison. (Reprinted with permission from[25]. © 2004 American Association for the Advancement of Science.)*

film, the calculated minimum conductivity $k_{min}$ of $Al_2O_3$, and diffuse mismatch model (DMM)[26] analysis of the $W/Al_2O_3$ nanolaminate are shown for comparison. As clearly seen, the thermal conductivity of the $W/Al_2O_3$ nanolaminate is lower than any other data.

## Correlated scattering

Correlated phonon scattering occurs when there is far-field interference of scattered phonons because of phase differences[18]. Scattering can be correlated in nanostructured materials. As Prasher[18] suggested, when the distance between nanoparticles embedded in a material is comparable to the phonon wavelength, then scattering can be phase correlated. Therefore, one can manipulate the phonon mean free path by adjusting the inter-nanoparticle distance. Correlated scattering could also be important in nanowires. For example, the thermal conductivity of a thin 22 nm Si nanowire measured by Li *et al.*[16] shows an unusual linear temperature dependence of thermal conductivity that cannot be explained by uncorrelated scattering[27], but could be explained by correlated scattering[28]. Murphy and Moore[28] have numerically studied effects of coherence between multiple scattering events and found this linear temperature dependence in model systems. Their calculations also predict that phonon localization could occur in narrower wires (less than 10 nm in diameter). Phonon localization occurs when correlated scattering events prevent a phonon from propagating and participating in thermal transport even though that phonon is excited. To study localization, measurements of heat capacity would offer extra insight because they could verify the existence of localized phonon modes that are excited, but not transported.

## Phonon filtering

Phonon filters prevent a spectral band(s) of phonons from propagating. The phonon-filtering effect was first demonstrated by Narayanamurti *et al.*[29] in 1979. They showed selective transmission of high-frequency phonons at low temperature using $GaAs/Al_{0.5}Ga_{0.5}As$ superlattices. In the superlattice, phononic band gaps eliminate transmission of phonons that satisfy the Bragg condition. This approach provides a good way of preventing narrow bands of phonons from propagating (i.e. those that satisfy the Bragg condition). To improve insulation, phonon filters that prevent a wide band of phonons from propagating should be used. This can be done by using the spectral aspect of interface thermal transport.

Interface thermal conductance is defined as $G = q/\Delta T$ where $q$ is the heat flux normal to the interface and $\Delta T$ is the temperature difference across the interface. The interface thermal conductance of metal-metal junctions[30] has a strong electronic contribution and is not discussed in this review. Prior to recent work[31,32], measured values of $G$ fell within a narrow range at room temperature[33-36], approximately $30\ MW/m^2K < G < 175\ MW/m^2K$.

To create insulating interfaces, the dissimilarity in vibrational spectra of the interfacing materials should be maximized. This causes

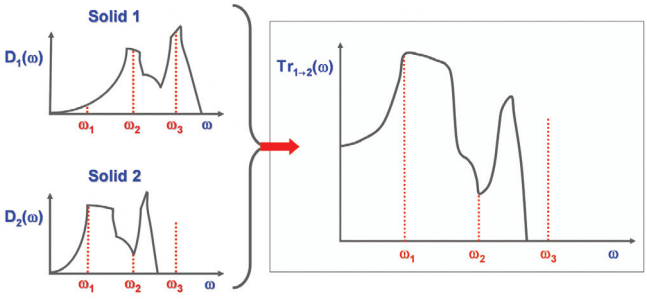


*Fig. 4 Illustration of phonon transmission probability as predicted by the DMM[26]. Given two interfacing solids 1 and 2 with vibrational spectra $D_1(\omega)$ and $D_2(\omega)$, the phonon transmission probability from 1 to 2, $Tr_{1\to2}(\omega)$, is dependent on the ratio of the spectra as shown. Representative locations of maxima and minima in the transmission probability are labeled on $D_1(\omega)$, $D_2(\omega)$, and $Tr_{1\to2}(\omega)$. The transmission probability at $\omega_3$ is zero because solid 2 does not vibrate at that frequency. Since only the lower frequency phonons are transmitted, $Tr_{1\to2}(\omega)$ is representative of a low-pass phonon filter.*

a lack of spectral coupling and minimizes the probability of phonon transmission across the interface. This effect is described by the diffuse mismatch model[26], which predicts the phonon transmission probability as a function of phonon frequency (Fig. 4). The dissimilarity in vibrational spectra is approximately proportional to the Debye temperature ratio of the interfacing materials. Lyeo and Cahill[32] used materials with Debye temperature ratios of 5-20 to create interfaces with $8\ MW/m^2K < G < 30\ MW/m^2K$. Fig. 5 shows the current range of interface thermal conductance, which incorporates this new lower limit. The new upper limit on interface thermal conductances (discussed in the 'Spectral Matching' section) is also shown.

This spectral aspect of interfacial thermal transport suggests insulating interfaces can be made by phonon filtering. Phonon filters can insulate because they prevent propagation of a certain phonon band(s). For example, consider the insulating interface between Pb and diamond[32,33]. The dominant portions of the Pb[37] and diamond[38] vibrational spectra are in the 1-2 THz and 50-80 THz ranges, respectively. The interface is insulating because the diamond reflects the low-frequency phonons of the Pb, and the Pb reflects the high-frequency phonons of the diamond. Hence, Pb can be used as a low-pass filter and diamond can be used as a high-pass filter. It should be noted that in spectrally mismatched solids, the filtering of phonons is not perfect, since anharmonic scattering enhances phonon transmission. This is demonstrated by the fact that the measured[32] Bi-diamond interface thermal conductance is greater than the radiation limit (Fig. 5). The radiation limit is the maximum possible interface conductance for a purely harmonic transport process involving one incoming and one outgoing phonon.

The existence of high- and low- pass phonon filters lead one to ask: are other types of filters possible? A type of interface that may exhibit band-pass filtering is that of a molecular junction. A molecular junction can consist of a self-assembled monolayer (SAM) sandwiched in between two solids (Fig. 6). Wang *et al.*[39] measured the thermal

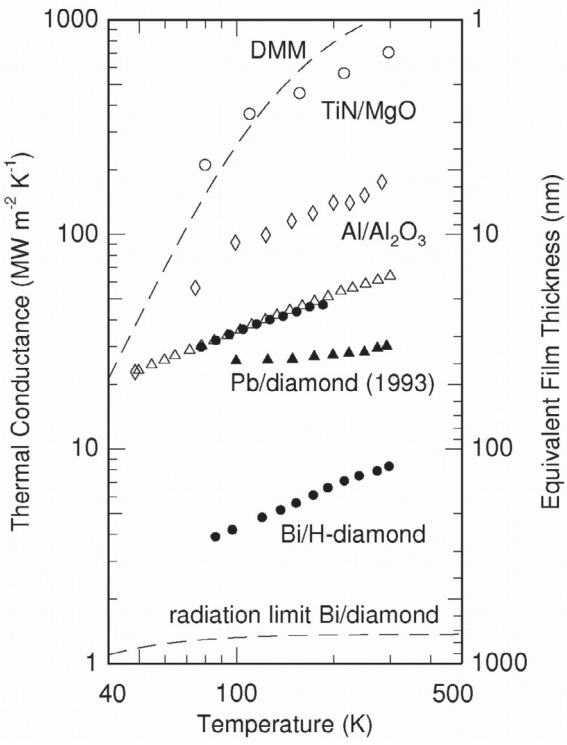


*Fig. 5 Thermal conductance of solid-solid interfaces. The right-hand axis gives the equivalent thickness of a thin film with a thermal conductivity of 1 W/mK that has the same thermal resistance as these single interfaces. Data are taken from the following: TiN/MgO, open circles[31]; Al/$Al_2O_3$, open diamonds[33]; Pb/diamond, filled triangles[33]; GST/ZnS:$SiO_2$, open triangles[35]; Al-oxide-Si structures, filled circles[36]; Bi/hydrogen-terminated-diamond, filled circles[32]. The dashed line labeled 'DMM' is a theoretical calculation of the TiN/MgO interface conductance using a modification of the DMM[31]. (Reprinted with permission from[32]. © 2006 American Physical Society.)*

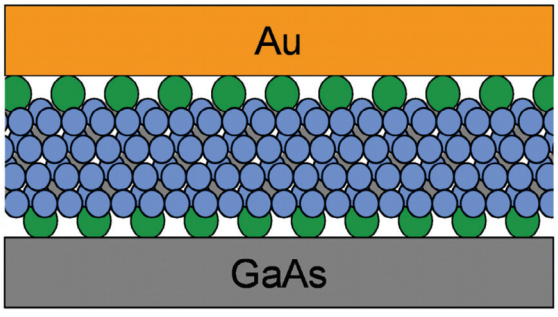


*Fig. 6 A molecular junction consisting of an alkanedithiol SAM sandwiched in between solid contacts of Au and GaAs. Sulfur, carbon, and hydrogen atoms are represented by green, gray, and blue, respectively. The bonds along the chain are strong covalent bonds whereas the lateral intermolecular bonds are weak van der Waals interactions. This molecular junction could exhibit band-pass phonon filtering and polarizing effects.*

conductance of Au/GaAs junctions with an interfacial alkanedithiol SAM. Even though the Debye temperature ratio of Au/GaAs is only ~2, the junction was insulating with $G$ ~ 25 MW/$m^2$K. Considering that other junctions[40] with Debye temperature ratios of 2 have G ~ 100-200 MW/$m^2$K, this molecular junction has a very low thermal conductance. This is likely to be caused by the SAM, which has a discrete vibrational spectrum of narrow bands[41]. In contrast, Au[42] and GaAs[43] have a continuous broadband vibrational spectrum. In this type of interface, only phonons that are resonant with the SAM's discrete vibrational spectra should transmit. Hence, the SAM acts as a band-pass filter.

In addition, molecular junctions such as SAMs should exhibit a phonon-polarizing effect because of a contrast in bond strengths[39]. The lateral intermolecular bonds in a SAM are the result of weak van der Waals interactions, whereas the Au and GaAs contain strong metallic and covalent bonds, respectively. In contrast, the bonds along the alkane backbone are covalent and similar in strength to the Au and GaAs bonds. Thus, the transverse vibrational frequencies of the SAM will be much lower than those of Au and GaAs, whereas the longitudinal frequencies will be similar. This should cause preferential transmission of longitudinal vibrations and create a polarizing effect.

Diamondoids are a type of nanostructure that should exhibit strong phonon-filtering effects. Fig. 7 shows some of the structures of diamondoids, which are well-defined hydrogen-terminated diamond crystals about 1 nm in size[44]. Adamantane ($C_{10}H_{16}$) is the smallest diamondoid and has a carbon framework that consists of a single cage-shaped structure. Larger diamondoids consist of multiple carbon cages that are face-fused together and come in a diverse set of geometries and sizes. Since the diamondoid surface is hydrogen-terminated, diamondoids interact with each other through weak van der Waals forces. The vibrations inside a diamondoid occur at very high frequencies (>10 THz) and are localized inside each structure. On the other hand, because of the weak van der Waals interaction, the surface vibrational frequencies should be on the order of 1 THz. This large mismatch should filter out much of the phonon spectra, thus producing very low thermal conductivity. The room temperature thermal conductivity of adamantane[45] is 0.2 W/mK and is comparable to the insulating limits of solids. Thermal conductivity data of larger diamondoids and/or diamondoid mixtures have yet to be reported. However, these diamondoids should behave similarly to solid $C_{60}$, which is also a van der Waals crystal with localized vibrations in the $C_{60}$ molecules. The room temperature thermal conductivity is 0.4 W/mK for a $C_{60}$ single crystal[46]. Reports[47,48] on the room temperature thermal conductivity of compressed $C_{60}$ powder have found values of 0.1 W/mK and 0.2 W/mK.

In addition to spectral mismatch, the interfacial bond strength also has an effect on thermal conductance. This has been observed[49,50] and simulated[50-52] at solid-liquid interfaces. Ge *et al.*[49] measured the interface thermal conductance of Au-SAM-$H_2O$ and Al-SAM-$H_2O$ interfaces, where the SAM was either hydrophobic or hydrophilic. They found that using hydrophilic SAMs increased the conductance by a factor of 2-3 compared with hydrophobic SAMs.

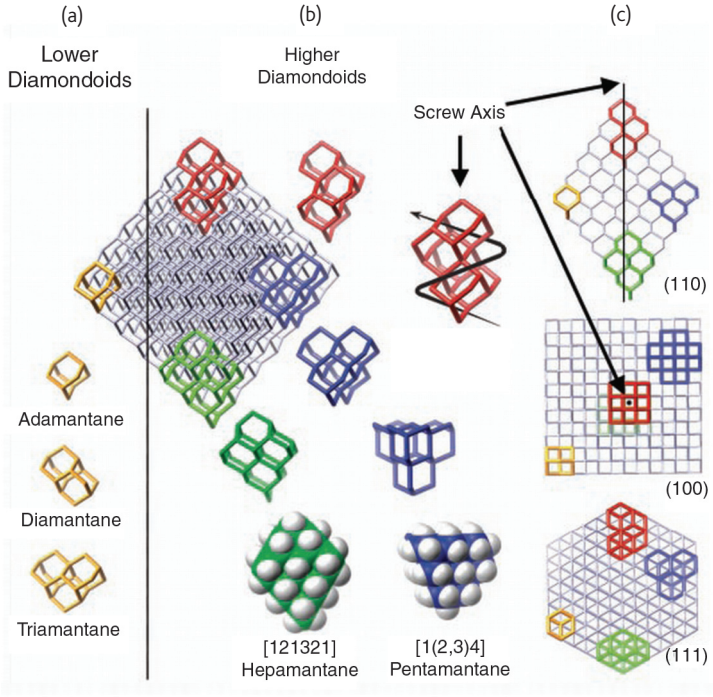


*Fig. 7 The relationship between the face-centered cubic diamond lattice and diamondoid structures. (a) Adamantane (yellow) is shown superimposed upon the lattice of a 455-carbon octahedral diamond (some carbons removed for clarity). Adamantane, diamantine, and triamantane (all in yellow) are also shown separately from the diamond lattice. (b) Screw-shaped pentamantane (red), pyramidal pentamantane (blue), and rhombus-shaped heptamantane (green) superimposed upon the diamond lattice and also separate from the lattice. (c) The 455-carbon diamond with superimposed diamondoid structures viewed along the (110), (100), and (111) lattice planes showing the diamond lattice faces of the pentamantanes and heptamantane. Views of the red pentamantane screw axis are indicated by straight arrows. The clockwise helical arrow indicates the groove in the screw-shaped pentamantane molecule. Because of their unique structure, diamondoids should exhibit strong phonon-filtering effects. (Reprinted with permission from[44]. © 2003 American Association for the Advancement of Science.)*

## The thermally conducting limit

In this section, we review work that pushes the conducting limits in thermal transport. For example, carbon nanotubes (CNTs) have already beaten the bulk limit of thermal conductivity. Experimental demonstrations of phonon waveguiding and ballistic phonon transport are also discussed.

### Beyond diamond – carbon nanotubes

Prior to the emergence of CNTs, diamond was regarded as the highest thermal conductor. Diamond's stiff $sp^3$ bonds result in a high phonon velocity and make monocrystalline diamond one of the best thermal conductors[53]. The room temperature thermal conductivity of naturally abundant diamond[54] is about 2300 W/mK, although that of isotopically pure diamond[55] is 3320 W/mK. CNTs possess a unique combination of properties that make them ideal thermal conductors. First, the carbon atoms in CNTs are bonded by $sp^2$ bonds, which are even strong than the $sp^3$ bonds in diamond[56]. Thus phonon velocities are greater in CNTs than in diamond. Second, because of its seamless tubular structure, phonon boundary scattering is absent in CNTs. A remarkably high thermal conductance in CNTs has been calculated theoretically[56,57] and demonstrated experimentally[58-63].

Before reviewing the thermal conductivity of individual CNTs, it should be mentioned that there is significant scatter in experimental data between different research groups. This is especially true for multiwalled CNTs (MWNTs), where the data can vary by up to one order of magnitude. The fact that thermal conductivity can be affected by growth parameters[9] might explain this. Fig. 8 shows the thermal conductivities of an individual MWNT[61] and an individual single-walled[63] carbon nanotube (SWNT). Pop *et al.*[62] also measured SWNT thermal conductivity and found it to be 3500 W/mK at room temperature, which is the highest room temperature value ever reported. The room temperature thermal conductivity of an MWNT is 3128 W/mK and is higher than that of naturally abundant diamond[54]. Although this is slightly less than isotopically pure diamond[55], that comparison may be irrelevant since the isotope content of the MWNTs[61] was not measured.

Given the exceptionally large conductance of CNTs, many researchers have tried to address whether thermal transport in CNTs is ballistic or diffusive. At present, the answer to this question is still unclear. The SWNT measurement by Yu *et al.*[63] is very close to the calculated ballistic result for a 1 nm-diameter SWNT and shows no characteristics of phonon-phonon umklapp scattering from 110-300 K. However, because of uncertainty in the SWNT diameter, partially diffusive transport cannot be ruled out. In the case of MWNTs, recent studies[64,65] have observed ballistic transport. However, data from Kim *et al.*[61] show an umklapp scattering peak, which is indicative of

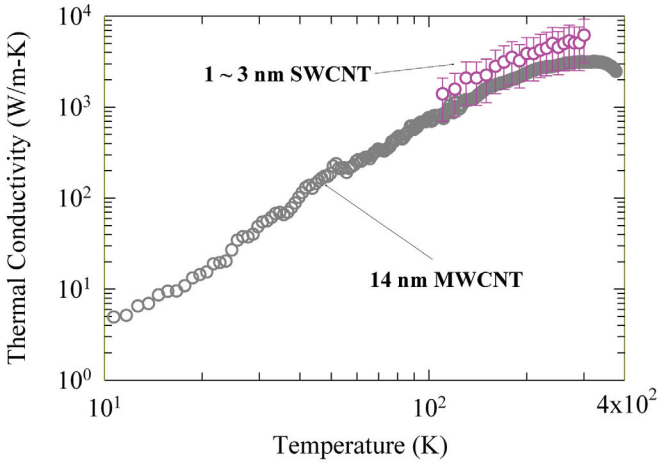


*Fig. 8 Thermal conductivities of an individual MWNT[61] and an individual SWNT[63]. An uncertainty in the SWNT diameter creates a large uncertainty in the SWNT thermal conductivity. (Reprinted with permission from[61] and [63]. © 2001 American Institute of Physics. © 2005 American Chemical Society.)*

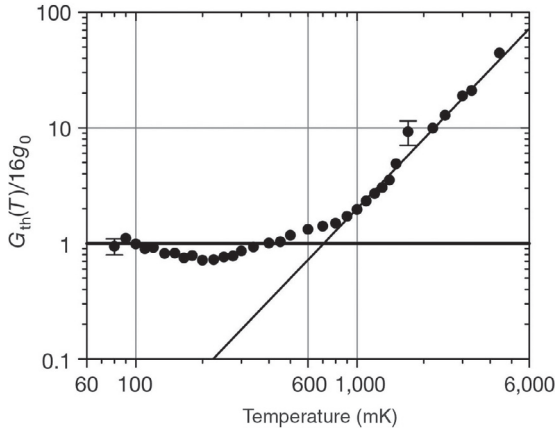


*Fig. 9 Measurement of the quantum of thermal conductance $g_0$. The thermal conductance of the test structure is denoted by $G_{th}$. The test structure consists of four phonon waveguides and a central heating region. (Reprinted with permission from[68]. © 2000 Macmillan Publishers Ltd.)*

diffusive transport. Despite the ongoing debate on whether or not phonon transport is ballistic in CNTs, this material seems to be a potential candidate for phonon waveguiding.

Polymer nanocomposites containing CNTs have been suggested as a practical way of utilizing the high thermal conductivity of individual CNTs[66]. However, the extremely small thermal conductance of the CNTs-polymer interface[50] is currently the biggest bottleneck in using CNTs as a material for high-performance thermal management systems.

## The quantum of thermal conductance

The quantum of thermal conductance $g_o$ is the maximum possible value of thermal energy transported per phonon mode in a one-dimensional system[67]. The thermal conductance quantum is given by $g_0 = (\pi^2 k_B^2/3h)T$, where $k_B$ and $h$ are the Boltzmann and Planck constants, respectively. As shown in the expression, the quantum of thermal conductance is linearly dependent on temperature with slope $\pi^2 k_B^2/3h \approx 1$ pW/K$^2$.

The first measurement of the quantum of thermal conductance was reported by Schwab *et al.*[68] in 2000. The thermal conductance data is shown in Fig. 9 and is normalized by 16 $g_0$. 16 $g_0$ is physically significant because in this experiment[68], there are four phonon waveguides, each of which has four occupied modes in the low-temperature limit. These four occupied modes correspond to one dilatational, one torsional, and two flexural degrees of freedom[68]. As shown in Fig. 9, the measured low temperature thermal conductance matches with the quantum of thermal conductance.

## Spectral matching

To maximize interface conductance, materials with similar Debye temperatures and minimal intrinsic defects should be used. This was done by Costescu *et al.*[31], who measured the thermal conductance of epitaxial TiN/MgO(001), TiN/MgO(111), and TiN/$Al_2O_3$(0001) junctions. Because these materials have similar Debye temperatures, the phonon-filtering effect should be minimized. In addition, defects in the substrate and film were minimized by careful fabrication procedures[31]. However, because of lattice mismatch and crystal orientations, the interfaces were expected to have varying amounts of misfit dislocations and stacking faults. For all three interfaces, the measured $G$ was approximately 700 MW/m$^2$K. It is surprising that stacking faults and misfit dislocations do not appear to have an effect on $G$. This may be an indication of other effects dominating $G$.

Majumdar and Reddy[69] have suggested that for metal-nonmetal interfaces, the limiting conductance could be an electron-phonon coupling conductance in the metal. This arises because electrons dominate thermal transport in a metal, but only phonons can carry heat across a metal-nonmetal interface. Thus the interface thermal transport becomes a two-step process: first, energy transfers from the metal electrons to the metal phonons; and second, energy transfers from the metal phonons to the nonmetal phonons. Majumdar and Reddy compared their theoretical analysis with the TiN/MgO data[31] and found good agreement[69].

## Conclusions

This article has reviewed how limits in thermal transport can be broken by nanostructuring. In the thermally insulating limit, we discussed how spectrally dependent scattering has been used to beat the alloy limit. This was accomplished in both nanowires and an alloy with epitaxially embedded nanoparticles. By using a high interface density, the amorphous limit has also been beaten. Additionally, data on the thermal conductivity of a thin Si nanowire show a linear temperature dependence which may be indicative of correlated scattering.

Solid-solid junctions that exhibit high- and low-pass phonon filtering have been discussed. Furthermore, the low conductance of SAM interfaces may be indicative of band-pass phonon filtering. SAMs should also have a polarizing effect because of differences in inter- and intramolecular bond strengths. Diamondoids are another type of nanostructure that should exhibit strong phonon filtering effects.

In the thermally conducting limit, CNTs have been shown to beat the bulk limit of thermal conductivity. Despite the ongoing debate on whether or not phonon transport is ballistic in CNTs, CNTs seem to be a potential candidate for phonon waveguiding. Observation of the thermal conductance quantum opens up the possibility for extremely high thermal conductances. Lastly, spectral matching is suggested to enhance interface thermal conductance. nt

## Acknowledgments

*This work was supported by the Basic Energy Sciences, Department of Energy, and the Chemical and Transport Systems Division of the National Science Foundation (NSF) and Office of Naval Research Multidisciplinary University Research Initiative grant (N00014-03-1-0790). RW gratefully acknowledges an NSF IGERT fellowship.*

### REFERENCES


1 Chu, R. C., *et al.*, *IEEE Trans. Device Mater. Reliab.* (2004) **4**, 568
2 McDaniel, T. W., *J. Phys.: Condens. Matter* (2005) **17**, R315
3 Figge, S., *et al.*, *Phys. Status Solidi A* (2003) **200**, 83
4 Padture, N. P., *et al.*, *Science* (2002) **296**, 280
5 Schelling, P. K., *et al.*, *Materials Today* (2005) **8** (6), 30
6 Majumdar, A., *Science* (2004) **303**, 777
7 Tien, C. L., *et al.*, *Microscale energy transport*. Taylor & Francis, Washington, D.C., (1998)
8 Majumdar, A., *J. Heat Transfer - Trans. ASME* (1993) **115**, 7
9 Cahill, D. G., *et al.*, *J. Appl. Phys.* (2003) **93**, 793
10 Cahill, D. G., *et al.*, *J. Heat Transfer - Trans. ASME* (2002) **124**, 223
11 Capinski, W. S., *et al.*, *Phys. Rev. B* (1999) **59**, 8105
12 Venkatasubramanian, R., *Phys. Rev. B* (2000) **61**, 3091
13 Li, D. Y., *et al.*, *Appl. Phys. Lett.* (2003) **83**, 3186
14 Harman, T. C., et al., *Science* (2002) **297**, 2229
15 Kim, W., *et al.*, *Phys. Rev. Lett.* (2006) **96**, 045901
16 Li, D. Y., *et al.*, *Appl. Phys. Lett.* (2003) **83**, 2934
17 Kim, W., and Majumdar, A., *J. Appl. Phys.* (2006) **99**, 084306
18 Prasher, R. S., *J. Heat Transfer - Trans. ASME* (2006) **128**, 627
19 Prasher, R. S., *J. Heat Transfer - Trans. ASME* (2004) **126**, 793
20 Jeng, M.-S., *et al.*, *Monte Carlo simulation of thermoelectric properties in nanocomposites*. Presented at the 24th International Conference on Thermoelectrics (IEEE), Clemson, SC, 2005
21 Prasher, R., *J. Appl. Phys.* (2006) **100**, 034307
22 Yang, R. G., and Chen, G., *Phys. Rev. B* (2004) **69**, 195316
23 Yang, R. G., *et al.*, *Phys. Rev. B* (2005) **72**, 125418
24 Kim, W., *et al.*, *unpublished results*
25 Costescu, R. M., *et al.*, *Science* (2004) **303**, 989
26 Swartz, E. T., and Pohl, R. O., *Rev. Mod. Phys.* (1989) **61**, 605
27 Mingo, N., *et al.*, *Nano Lett.* (2003) **3**, 1713
28 Murphy, P. G., *et al.*, *unpublished results*
29 Narayanamurti, V., *et al.*, *Phys. Rev. Lett.* (1979) **43**, 2012
30 Gundrum, B. C., *et al.*, *Phys. Rev. B* (2005) **72**, 245426
31 Costescu, R. M., *et al.*, *Phys. Rev. B* (2003) **67**, 054302
32 Lyeo, H. K., and Cahill, D. G., *Phys. Rev. B* (2006) **73**, 144301
33 Stoner, R. J., *et al.*, *Phys. Rev. B* (1993) **48**, 16373
34 Smith, A. N., and Maris, H. J., *Microscale Thermophys. Eng.* (2000) **4**, 51
35 Kim, E.-K., *et al.*, *Appl. Phys. Lett.* (2000) **76**, 3864
36 Cahill, D. G., *et al.*, *High Temperatures-High Pressures* (2000) **32**, 135
37 Brockhouse, B. N., *et al.*, *Phys. Rev.* (1962) **128**, 1099
38 Warren, J. L., *et al.*, *Phys. Rev.* (1967) **158**, 805
39 Wang, R. Y., *et al.*, *Appl. Phys. Lett.* (2006) **89**, 173113
40 Stevens, R. J., *et al.*, *J. Heat Transfer - Trans. ASME* (2005) **127**, 315
41 Porter, M. D., *et al.*, *J. Am. Chem. Soc.* (1987) **109**, 3559
42 Lynn, J. W., *et al.*, *Phys. Rev. B* (1973) **8**, 3493
43 Waugh, J. L. T., and Dolling, G., *Phys. Rev.* (1963) **132**, 2410
44 Dahl, J. E., *et al.*, *Science* (2003) **299**, 96
45 Wigren, J., *et al.*, *Mol. Cryst. Liq. Cryst.* (1980) **59**, 137
46 Yu, R. C., *et al.*, *Phys. Rev. Lett.* (1992) **68**, 2050
47 Olson, J. R., *et al.*, *Science* (1993) **259**, 1145
48 Withers, J. C., *et al.*, *J. Am. Ceram. Soc.* (1993) **76**, 754
49 Ge, Z. B., *et al.*, *Phys. Rev. Lett.* (2006) **96**, 186101
50 Huxtable, S. T., *et al.*, *Nat. Mater.* (2003) **2**, 731
51 Barrat, J.-L., and Chiaruttini, F., *Mol. Phys.* (2003) **101**, 1605
52 Shenogin, S., *et al.*, *Appl. Phys. Lett.* (2004) **85**, 2229
53 Wei, L. H., *et al.*, *Phys. Rev. Lett.* (1993) **70**, 3764
54 Onn, D. G., *et al.*, *Phys. Rev. Lett.* (1992) **68**, 2806
55 Anthony, T. R., *et al.*, *Phys. Rev. B* (1990) **42**, 1104
56 Berber, S., *et al.*, *Phys. Rev. Lett.* (2000) **84**, 4613
57 Mingo, N., and Briodo, D. A., *Phys. Rev. Lett.* (2005) **95**, 096105
58 Chang, C. W., *et al.*, *Phys. Rev. Lett.* (2006) **97**, 085901
59 Choi, T.-Y., *et al.*, *Nano Lett.* (2006) **6**, 1589
60 Fujii, M., *et al.*, *Phys. Rev. Lett.* (2005) **95**, 065502
61 Kim, P., *et al.*, *Phys. Rev. Lett.* (2001) **87**, 215502
62 Pop, E., *et al.*, *Nano Lett.* (2006) **6**, 96
63 Yu, C. H., *et al.*, *Nano Lett.* (2005) **5**, 1842
64 Brown, E., *et al.*, *Appl. Phys. Lett.* (2005) **87**, 023107
65 Chiu, H.-Y., *et al.*, *Phys. Rev. Lett.* (2005) **95**, 226101
66 Moniruzzaman, M., and Winey, K. I., *Macromolecules* (2006) **39**, 5194
67 Rego, L. G. C., and Kirczenow, G., *Phys. Rev. Lett.* (1998) **81**, 232
68 Schwab, K., *et al.*, *Nature* (2000) **404**, 974
69 Majumdar, A., and Reddy, P., *Appl. Phys. Lett.* (2004) **84**, 4768